Food and Chemical Toxicology 129 (2019) 281–290

Contents lists available at ScienceDirect

Food and Chemical Toxicology

journal homepage: www.elsevier.com/locate/foodchemtox

Activation of TRPC6 channels contributes to (+)-conocarpan-induced apoptotic cell death in HK-2 cells

Guoling Yang[1], Hui Ma[1], Yanliang Wu, Baoping Zhou, Chunlei Zhang, Chengzhi Chai**, Zhengyu Cao*

State Key Laboratory of Natural Medicines & Jiangsu Provincial Key Laboratory of TCM Translational Research, School of Traditional Chinese Pharmacy, China Pharmaceutical University, Nanjing, Jiangsu, 211198, China

ARTICLE INFO

Keywords:
Apoptosis
Ca^{2+}
Caspase
Conocarpan
TRPC6

ABSTRACT

(+)-Conocarpan (CNCP), a neolignan frequently found in many medicinal and edible plants displays a broad spectrum of bioactivity. Here, we demonstrated that CNCP induced apoptotic cell death in human kidney-2 (HK-2) cells in a concentration-dependent manner (IC_{50} = 19.3 μM) and led to the sustained elevation of intracellular Ca^{2+} ($[Ca^{2+}]_i$). Lower extracellular Ca^{2+} concentrations from 2.3 mM to 0 mM significantly suppressed the CNCP-induced Ca^{2+} response by 69.1%. Moreover, the depletion of intracellular Ca^{2+} stores using thapsigargin normalized CNCP-induced Ca^{2+} release from intracellular Ca^{2+} stores, suggesting that the CNCP-induced Ca^{2+} response involved both extracellular Ca^{2+} influx and Ca^{2+} release from intracellular Ca^{2+} stores. SAR7334, a TRPC3/6/7 channel inhibitor, but neither Pyr3, a selective TRPC3 channel inhibitor, nor Pico145, a TRPC1/4/5 inhibitor, suppressed the CNCP-induced Ca^{2+} response by 57.2% and decreased CNCP-induced cell death by 53.4%, suggesting a critical role for TRPC6 channels in CNCP-induced Ca^{2+} influx and apoptotic cell death. Further electrophysiological recording demonstrated that CNCP directly activated TRPC6 channels by increasing channel open probability with an EC_{50} value of 6.01 μM. Considered together, these data demonstrate that the direct activation of TRPC6 channels contributes to CNCP-induced apoptotic cell death in HK-2 cells. Our data point out the potential risk of renal toxicity from CNCP if used as a therapeutic agent.

1. Introduction

Lignans and neolignans are a large group of naturally occurring polyphenols derived from the oxidative coupling of two C6–C3 units (Teponno et al., 2016). Lignans and neolignans are frequently found in a variety of medical plants including *Linum, Anthriscus,* and *Podophyllum,* as well as edible plants including flaxseed, sesame (Pedaliaceae), cereal products (Poaceae or Gramineae), and *Brassica* vegetables (Brassicaceae) (Cao et al., 2015; Kim et al., 2010; Rizwan et al., 2014; Stojakowska et al., 2013; Teponno et al., 2016). Lignans possess a variety of pharmacological activities such as having anti-viral (Parhira et al., 2014) and anti-inflammatory properties (Gao et al., 2018) and neuroprotective activity (Chen et al., 2016; Jeong et al., 2013), and they also have beneficial effects related to the prevention of cardiovascular diseases (Giglio et al., 2018), as well as nephropathies (Ma et al., 2013; Rizwan et al., 2014; Zuniga-Toala et al., 2013).

(+)-Conocarpan (CNCP) is a benzofuran neolignan and was first isolated from *Conocarpus erectus* (Hayashi and Thomson, 1975). This compound was reported to occur in a number of medical plants, including *Piper regnellii* (Felipe et al., 2006; Pessini et al., 2003), *Krameria lappacea* (Baumgartner et al., 2011a, 2011b), *Krameria triandra* (Carini et al., 2002) and *Piper solmsianum* (Da Silva et al., 2010). CNCP is a main active compound of *K. lappacea* (Baumgartner et al., 2011a), a drug listed in the European Pharmacopoeia, and can reach levels as high as 0.71% in the roots. The concentrations of CNCP in the leaves, stems and roots of *P. regnellii* are high, reaching 0.72%, 0.79% and 0.84%, respectively (Felipe et al., 2006). CNCP has been reported to have insecticidal (Chauret et al., 1996), anti-fungal (De Campos et al., 2005), anti-trypanosomal (Luize et al., 2006), anti-tuberculotic (Scodro et al., 2013), photoprotective (Carini et al., 2002), antinociceptive and

* Corresponding author. Jiangsu Provincial Key Laboratory for TCM Evaluation and Translational Research, School of Traditional Chinese Pharmacy, China Pharmaceutical University, Nanjing, Jiangsu, 211198, China.
** Corresponding author. Jiangsu Provincial Key Laboratory for TCM Evaluation and Translational Development, China Pharmaceutical University, Nanjing, Jiangsu, 211198, China.
E-mail addresses: chaichengzhi@126.com (C. Chai), zycao1999@hotmail.com (Z. Cao).
[1] Equal contribution.

https://doi.org/10.1016/j.fct.2019.04.061
Received 16 January 2019; Received in revised form 25 April 2019; Accepted 30 April 2019
Available online 03 May 2019

Abbreviations

CNCP	(+)-conocarpan
$[Ca^{2+}]_i$	intracellular Ca^{2+} concentration
HK-2	human kidney 2
FBS	foetal bovine serum
FDA	fluorescein diacetate
OAG	1-oleoyl-2-acetyl-sn-glycerol
PI	propidium iodide
P_o	open probability
RT	room temperature
RDP	*Ribes diacanthum* Pall
RMK	*Ribes manshuricum* (Maxim.) Kom
TG	thapsigargin
TRPC	transient receptor potential canonical

anti-inflammatory activities (Da Silva et al., 2010). The topical anti-edematous activity of CNCP occurs through the inhibition of NFκB, cyclooxygenases, 5-lipoxygenase and microsomal prostaglandin E2 synthase-1 (Baumgartner et al., 2011b). Due to its broad activities, CNCP has been synthesized by several groups (Chen and Weisel, 2013; Silva et al., 2018; Zheng et al., 2003).

Our previous investigation on the chemical constitutes of *Ribes diacanthum* Pall (RDP) and another related species, *Ribes manshuricum* (Maxim.) Kom (RMK) identified a total of 50 compounds including phenolic acids, anthocyanins, flavonoids and neolignans (Li et al., 2018; Zhou et al., 2016). RDP, a Mongolian folk medicine, is widely used for treating diseases of the urinary system such as bladder diseases, cystitis, kidney stones, and edema (Ligaa, 2006). We demonstrated that RDP aqueous extract displays protective effects on cisplatin-induced kidney injury (Tilyek et al., 2016) and unilateral ureteral occlusion-induced kidney fibrosis (Gu et al., 2018). Previous efforts to discover nephroprotective components identified two acylated β-hydroxynitrile glycosides, ribemansides A and B, that suppress the fibrogenesis of human kidney-2 (HK-2) cells and inhibit the activity of transient receptor potential canonical 6 (TRPC6) channels (Zhou et al., 2018). However, mice receiving a high dose of RDP crude extract (1000 mg/kg/d, *ig.*) for 28 consecutive days displayed significantly increased levels of blood urea nitrogen and serum creatinine, suggesting the existence of components in RDP crude extract that are potentially toxic to the kidney. Further analysis of the toxic components of RDP identified CNCP as a toxic agent that decreased cell viability in HK-2 cells.

In the present study, we investigated the toxic effect of CNCP and the mechanism by which CNCP induced cell death in HK-2 cells. We demonstrated that CNCP induces apoptotic cell death in HK-2 cells through the activation of caspase-3 pathway. We also demonstrated that CNCP persistently elevates intracellular Ca^{2+} concentration ($[Ca^{2+}]_i$). Further pharmacological investigation demonstrated that CNCP-induced Ca^{2+} response occurs through both extracellular Ca^{2+} influx mediated by TRPC6 channels and by Ca^{2+} release from intracellular Ca^{2+} stores. Electrophysiological recording demonstrated that CNCP directly activates TRPC6 channels with an EC_{50} value of 6.01 μM. These data demonstrate that the direct activation of TRPC6 channel contributes to CNCP-induced apoptotic cell death in HK-2 cells.

2. Materials and methods

2.1. Materials

(+)-Conocarpan (CNCP, CAS# 221,666-27-9) was purified from RDP as described previously, and the purity was accessed to be greater than 98% by HPLC (Zhou et al., 2016). Foetal bovine serum (FBS), 1-oleoyl-2-acetyl-sn-glycerol (OAG), thapsigargin (TG) and all of the inorganic chemicals were purchased from Sigma-Aldrich (St. Louis, MO, USA). HEPES, G418, RPMI 1640 medium, Earle's minimum essential medium, penicillin, and streptomycin were purchased from ThermoFisher Scientific (Waltham, MA, USA). The BCA Protein Assay kit was obtained from Beyotime Institute of Biotechnology (Nanjing, Jiangsu, China). The apoptosis detection kit, TRIzol reagent and the HiScript Q RT SuperMix for qPCR (+gDNA wiper) kits were purchased from Vazyme Biotech Co., Ltd. (Nanjing, Jiangsu, China). The primary antibody to caspase-3 was purchased from ProteinTech (Wuhan, Hubei, China). Anti-TRPC6 and anti-tubulin antibodies were purchased from Santa Cruz Biotechnology (Santa Cruz, CA, USA) and Bioworld technology Co. Ltd. (Nanjing, Jiangsu, China), respectively. The IRDye (680RD or 800CW)-labelled secondary antibodies were purchased from LI-COR Biotechnology (Lincoln, NE, USA). Hieff™ qPCR SYBR® Green Master Mix (Low Rox Plus) was obtained from Yeasen Biotechnology Co. Ltd. (Shanghai, China). SAR7334, Pico145 and Pyr3 were purchased from MedChemExpress Co. Ltd. (Shanghai, China).

2.2. HK-2 cell culture

Human proximal tubular cells (human kidney-2, HK-2) were generous gifts from Professor Bicheng Liu (Zhongda Hospital, Southeast University, Nanjing, China). HK-2 cells were cultured as previously described (Zhou et al., 2018). Briefly, cells were cultured in RPMI 1640 medium supplemented with 2 mg/mL NaHCO3, 10% FBS, 10 mM HEPES, 100 U/mL penicillin, and 0.1 mg/mL streptomycin at 37 °C in an atmosphere of 5% CO2 and 95% humidity. Cells at 70–80% confluency were digested with 0.05% trypsin and seeded in 96 well or 12 well plates (Corning; Corning, NY, USA) at densities of 6000 cells/well or 40,000 cells/well, respectively. Cells were cultured overnight before measuring CNCP-induced cell death.

2.3. TRPC6-HEK-293 cell culture

HEK-293 cells stably expressing mouse TRPC6 channels were a generous gift from Prof. Michael X. Zhu at the University of Texas Health Science Center at Houston. The cells were cultured in Earle's minimum essential medium supplemented with 10% FBS, 10 mM HEPES, 2 mM L-glutamine, 100 U/mL penicillin, 0.1 mg/mL streptomycin, and 200 μg/mL G418 at 37 °C in an atmosphere of 5% CO2 and 95% humidity. Cells cultured in T75 flasks (Corning, NY, USA) to approximately 80% confluence were digested with 0.05% trypsin and seeded in poly-D-lysine coated 96 well plates or 35 mm dishes (Corning) at densities of ~20,000 cells/well or 1000 cells/well, respectively. Cells were cultured for 6 h before Ca^{2+} imaging and patch clamp experiments.

2.4. Cell viability assay

A MTT assay was used to access cell viability. HK-2 cells cultured in 96 well plates were continuously exposed to CNCP in serum free medium for 24 h. Inhibitors were applied 30 min before addition of CNCP. After the removal of the medium, a volume of 100 μL of 0.5 mg/mL MTT was added to each well and incubated for an additional 4 h at 37 °C. Subsequently, supernatants were removed and a volume of 100 μL of DMSO was added to each well to dissolve formazan crystals that had formed. Absorbance was detected at 560 and 670 nm (reference wavelength), and the differences between both extinctions were calculated. Data were expressed as percentage of vehicle control (0.1% DMSO).

2.5. Fluorescein diacetate (FDA) and propidium iodide (PI) staining

FDA/PI staining was performed as described previously (He et al., 2017) to quantify cell death. After exposure to CNCP for the indicated lengths of time, HK-2 cells were stained by FDA (5 μg/mL) and PI (1 μg/mL) at RT for 5 min. Images were taken using a Nikon Eclips Ti–U inverted fluorescence microscope by using fluorescein isothiocyanate (FITC) and Texas Red filters and the number of live (green) and dead cells (red) were counted. Data were presented as percent dead cells.

2.6. Flow cytometry

Flow cytometry was used to detect cell apoptosis using a commercially available apoptosis detection kit. After vehicle (0.1% DMSO) and CNCP exposure, HK-2 cells were digested with 0.05% trypsin. After centrifugation for 5 min at 300 × *g*, cells were resuspended in binding buffer and incubated with a solution containing FITC-conjugated annexin-V and propidium iodide (PI) for 10 min. Fluorescence was detected using a MACSQuant flow cytometer (Miltenyi Biotec, Bergisch Gladbach, Germany). Percentage of apoptotic cells was calculated using FlowJo software (Version 10, BD™; FlowJo, LLC, Ashland, USA).

2.7. Intracellular Ca^{2+} concentration determination

The intracellular Ca^{2+} concentration was determined as described previously (Zou et al., 2017). Briefly, after incubation with 4 μM Fluo-4/AM (TEFlabs, Austin, TX, USA) at 37 °C for 50 min in the dark, the HK-2 cells were gently washed four times with Locke's buffer (in mM: HEPES 8.6, KCl 5.6, NaCl 154, D-glucose 5.6, $MgCl_2$ 1.0, $CaCl_2$ 2.3, and glycine 0.1, pH 7.4) and transferred to the chamber of a fluorescent imaging plate reader (FLIPR$^{Tetra®}$; Molecular Devices, Sunnyvale, CA). Basal fluorescence units (F_0) were recorded for 200 s followed by the addition of various concentrations of CNCP and the fluorescent signals (F) were continuously recorded for an additional 10 min. To determine the influence of TRPC inhibitors on CNCP, baseline fluorescence was measured for 25 s, after which inhibitors were added and fluorescence units were recorded for 75 s before the addition of CNCP. Data were presented as F/F_0 where F_0 was the basal fluorescence unit and F was the fluorescence unit at specific time point. The area under the curve (AUC) was used to quantify the CNCP Ca^{2+} response and the effect of inhibitors on CNCP induced Ca^{2+} response.

2.8. Electrophysiology recordings

HEK-293 cells stably expressing TRPC6 channels were seeded in 35 mm dishes for 6 h before the experiments were conducted. Whole cell and outside out patch recordings were performed at room temperature using an EPC-10 (HEKA Instruments Inc., Bellmore, NY) amplifier controlled by PatchMaster software (HEKA, Pfalz, Germany) as described previously (Qu et al., 2017). Recording pipettes were pulled from micropipette glass to 2–3 MΩ when filled with a pipette solution containing (in mM): 140 CsCl, 1 $MgCl_2$, 5 EGTA, and 10 HEPES, pH adjusted to 7.2 with CsOH and placed in a bath solution containing (in mM): 140 NaCl, 5 KCl, 2 $CaCl_2$, 1 $MgCl_2$, 10 glucose, and 10 HEPES, pH adjusted to 7.4 with NaOH. Cells were held at 0 mV and voltage ramps (300 ms) from −100 to +100 mV were applied every 1 s. Cells were continuously perfused with CNCP diluted in the bath solution through a press-driven multichannel system with the outlet placed approximately 50 μm away from the cell being recorded. All of the currents were recorded at 5 kHz.

2.9. Real-time quantitative PCR analysis

Cells were lysed and total RNA was extracted using TRIzol reagent. The concentration of RNA was analysed by measuring the ratio of optical density (260 nm/280 nm) using a nanodrop (Allsheng, Hangzhou, China). Reverse transcription of RNA was performed using the HiScript Q RT SuperMix for qPCR (+gDNA wiper) kit according to the manufacturer's protocol. Quantitative real time PCR (RT-PCR) was performed using Hieff™ qPCR SYBR® Green Master Mix (Low Rox Plus) with a QuantStudio 3 RT-PCR System (ThermoFisher Scientific, Waltham, MA). The quantification of mRNA expression levels was performed using $2^{-\Delta Ct}$ method, with the housekeeping gene, GAPDH, as a control. The primer sequences used in this study are listed in **Table 1**.

Table 1
Forward and reverse primers for qRT-PCR reactions.

Name	Forward Primers (5' – 3')	Reverse Primers (5' – 3')
hTRPC1	CACCTGTCATTTTAGCTGCTCATC	CCGGAGGCTATCCTTTTTGTT
hTRPC3	CAAGAATGACTATCGGAAGC	GCCACAAACTTTTTGACTTC
hTRPC4	AGGTACTCTGCCTACTCCCTTCAA	GCAGCTCGCCTCCCTATTG
hTRPC5	CCACCAGCTATCAGATAAGG	CGAAACAAGCCACTTATACCC
hTRPC6	TGAAGTGAAATCAGTGGTCA	AAATTTCCACTCCACATCAG
hTRPC7	CATAGCCTATTGGATTGCTC	GGTAGTCTGTGAAGGTTTCG
hGAPDH	GAAGGTGAAGGTCGGAGTCAAC	CAGAGTTAAAAGCAGCCCTGGT

2.10. Western blotting

Western blotting experiments were performed as described previously (Zou et al., 2017). Briefly, protein samples (30–40 μg) were loaded onto a 15% SDS-PAGE gel and then transferred to a nitrocellulose membrane. After electroblotting, the membranes were blocked with 5% nonfat milk in PBS for 1 h at RT and then subsequently incubated with primary antibodies overnight at 4 °C. The primary antibodies used were anti-caspase-3 (1:1000) and anti-TRPC6 (1:500). After washing, the membranes were incubated with IRDye (680RD or 800CW) labelled secondary antibodies (1:10,000) for 1 h at RT. Images were obtained by scanning the membranes using the LI-COR Odyssey Infrared Imaging System (LI-COR Biotechnology, Lincoln, NE). Densitometry was performed using LI-COR Odyssey Infrared Imaging System application software (version 2.1).

2.11. Statistical analysis

Graphing and statistical analysis were performed using GraphPad Prism software (Version 6.0, San Diego, CA). All data are expressed as the means ± S.E.M. Concentration response relationship curves were fit using a nonlinear equation using GraphPad Prism software (Version 6.0). Statistical significance between groups was calculated using an ANOVA and, where appropriate, a Dunnett's multiple comparison test. A p value less than 0.05 was considered to be statistically significant.

3. Results

3.1. CNCP induced cytotoxicity in HK-2 cells

The chemical structure of CNCP is shown in Fig. 1A. After exposure to CNCP, the cell viability was accessed by MTT assay. Fig. 1B shows that 24 h exposure decreased cell viability with an IC_{50} value of 19.3 μM (16.0–23.38 μM, 95% Confidence Intervals, 95% CI). FDA/PI staining also showed that CNCP exposure induced HK-2 cell death in a time dependent manner. Longer exposure induced more cell death. CNCP (30 μM) exposure for 1 h led to an 11.78% increase in cell death, and the levels gradually increased to be 17.83%, 19.63%, 27.98%, and 35.59% after 3, 6, 12 and 24 h exposure, respectively (Fig. 1D). To investigate whether CNCP also induced apoptotic cell death, cells were labelled with Annexin V-FITC/PI. Flow cytometry analysis showed that treatment with CNCP (10 and 30 μM) for 2 h significantly increased apoptotic cell death in HK-2 cells (Fig. 1E&F).

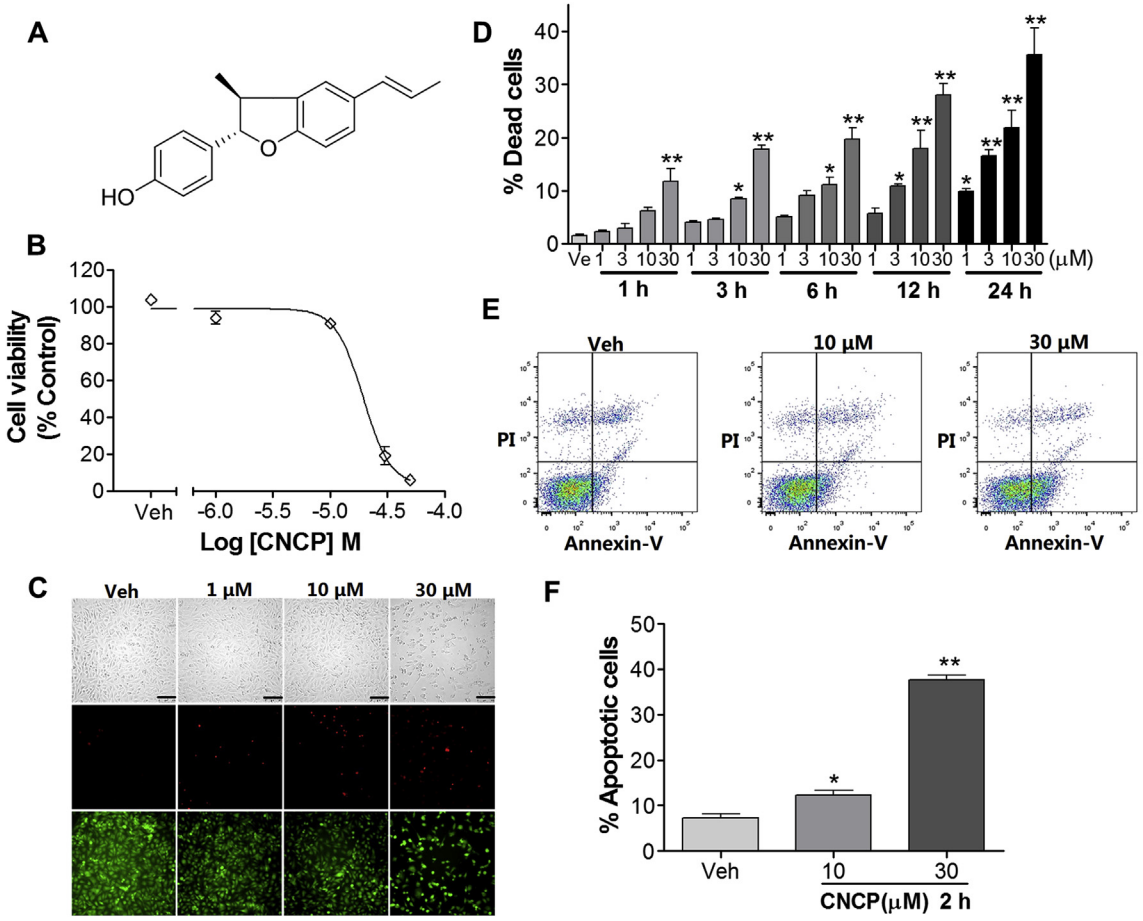

Fig. 1. CNCP induced cell death in HK-2 cells. (A) Chemical structure of CNCP. (B) Concentration-response relationship curve for CNCP exposure (24 h) induced cell death in HK-2 cells as measured by MTT assay. (C) Representative images for FDA and PI double stained HK-2 cells after exposure to vehicle (0.1% DMSO) or various concentrations of CNCP for 24 h. Scale bar = 100 μm. (D) Quantification of % dead cells measured by FDA and PI double staining after exposure to vehicle (0.1% DMSO) and different concentrations of CNCP for different time periods. (E) Representative flow cytometry diagrams in the presence or absence of CNCP. Apoptosis in HK-2 cells was detected by Annexin V-FITC/PI double staining and flow cytometry after exposure to vehicle (0.1% DMSO) or CNCP (10 μM and 30 μM). (F) Quantitation of apoptotic cells measured by flow cytometry. Each data point represents mean ± S.E.M. *, $p < 0.05$, **, $p < 0.01$, CNCP *vs.* vehicle. All experiments were repeated three times, each in triplicates.

3.2. CNCP led to elevated intracellular Ca^{2+} in HK-2 cells that involved both extracellular Ca^{2+} influx and intracellular Ca^{2+} release

The homeostasis of $[Ca^{2+}]_i$ regulates a variety of physiological responses, and $[Ca^{2+}]_i$ overloading is a major cause of cell death. We therefore investigated CNCP Ca^{2+} response in HK-2 cells using a Ca^{2+} specific fluorescence dye, Fluo-4/AM. The addition of CNCP produced a concentration-dependent elevation of $[Ca^{2+}]_i$. At 30 μM, CNCP produced a gradually increased Ca^{2+} response with a maximal response of less than 0.3 units ($\Delta F/F_0$). However, at concentrations greater than or equal to 50 μM, CNCP produced a rapid and robust elevation of $[Ca^{2+}]_i$ in HK-2 cells (Fig. 2A**&B**). To explore the Ca^{2+} source, the CNCP Ca^{2+} response was measured in the extracellular solutions with normal (2.3 mM) and decreased Ca^{2+} (0 mM, with 1 mM EGTA). Fig. 2C&D shows that replacement of the extracellular solution without Ca^{2+} reduced CNCP response by 69.1% suggesting that both extracellular Ca^{2+} influx and intracellular Ca^{2+} release were involved in CNCP-induced Ca^{2+} response. To further confirm the Ca^{2+} release from intracellular Ca^{2+} store as a factor of the observed CNCP-induced Ca^{2+} response, HK-2 cells were treated with thapsigargin (TG, 2 μM) in the extracellular solution without Ca^{2+} to deplete the intracellular Ca^{2+} store before challenging with CNCP (50 μM). The application of TG produced a transient elevation of $[Ca^{2+}]_i$ that recovered to basal level within 10 min (Fig. 2E). Pretreatment with TG abolished CNCP-induced Ca^{2+} response further demonstrating the role of Ca^{2+} release in the CNCP-induced Ca^{2+} response in HK-2 cells (Fig. 2E&F).

3.3. Transient receptor potential canonical (TRPC) channels were expressed in HK-2 cells

TRPCs are a class of Ca^{2+} permeable, nonselective cation channels expressed in many cell types (Abramowitz and Birnbaumer, 2009). The mutation of TRPC6 channels is associated with focal segmental glomerulosclerosis (FSGS) (Winn et al., 2005). Moreover, TRPC3 and TRPC6 KO mice display attenuated kidney fibrosis in a unilateral ureteral obstruction (UUO) mouse model (Saliba et al., 2015; Wu et al., 2017). We therefore examined whether TRPC channels were expressed in HK-2 cells. RT-PCR analysis showed the mRNA expression levels of TRPC1 and TRPC3-6 but not TRPC7 channels in HK-2 cells with rank order of TRPC1 > TRPC4 > TRPC6 > TRPC5 > TRPC3 (Fig. 3A). To validate the reliability of the primers used for detecting TRPC7, we analysed the TRPC7 expression in human keratinocyte cells. Keratinocytes showed marginal levels of TRPC7 mRNA expression (Fig. 3B). Further Western blot analysis showed that TRPC6 protein was expressed in HK-2 cells (Fig. 3C). The TRPC6 channel activator, OAG (Hofmann et al., 1999), elicited an elevation of $[Ca^{2+}]_i$ (Fig. 3D&E) albeit the response was smaller than that of CNCP (Fig. 2A). The OAG Ca^{2+} response in HK-2 cells was inhibited by the TRPC6 channel

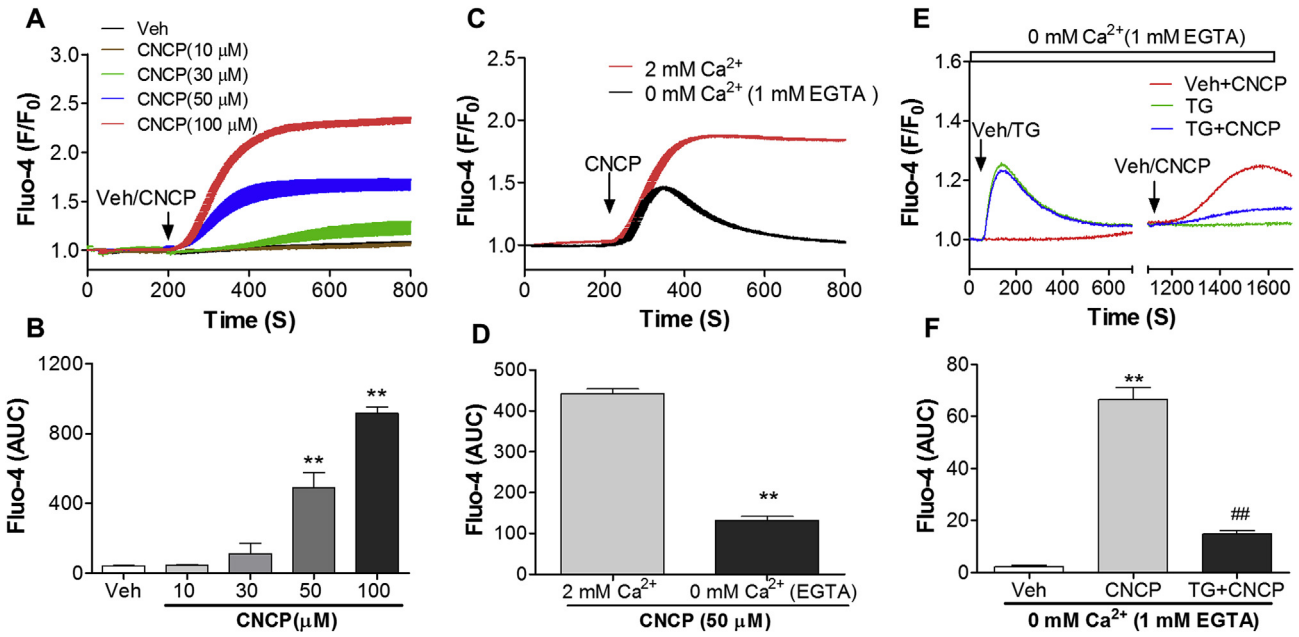

Fig. 2. Influence of CNCP on the elevation of intracellular Ca^{2+} concentration ($[Ca^{2+}]_i$) in HK-2 cells. (A) Representative trace of Ca^{2+} dynamics in the presence and absence of CNCP (10 μM, 30 μM, 50 μM and 100 μM) in HK-2 cells. (B) Quantitation of CNCP-induced Ca^{2+} response in HK-2 cells. **, $p < 0.01$, CNCP *vs.* vehicle. (C) Representative trace of Ca^{2+} dynamics induced by CNCP (50 μM) in HK-2 cells in Ca^{2+} free (1 mM EGTA) and normal Ca^{2+} (2.3 mM) extracellular solutions. (D) Quantification of CNCP Ca^{2+} response in extracellular solutions containing 0 mM or 2.3 mM Ca^{2+}. **, $p < 0.01$, 0 mM Ca^{2+} vs. 2.3 mM Ca^{2+} extracellular solution. (E) Representative trace of CNCP (50 μM) on $[Ca^{2+}]_i$ in the presence and absence of thapsigargin (TG, 2 μM) in a Ca^{2+} free extracellular solution in HK-2 cells. (F) Quantification of CNCP effects on $[Ca^{2+}]_i$ after depletion of intracellular Ca^{2+} store. Area under curve (AUC) values were from an epoch of 10 min from addition of CNCP. **$p < 0.01$, CNCP *vs.* vehicle, ##, $p < 0.01$, TG + CNCP *vs.* CNCP. All experiments were repeated three times with similar results. Each data point represents mean ± S.E.M.

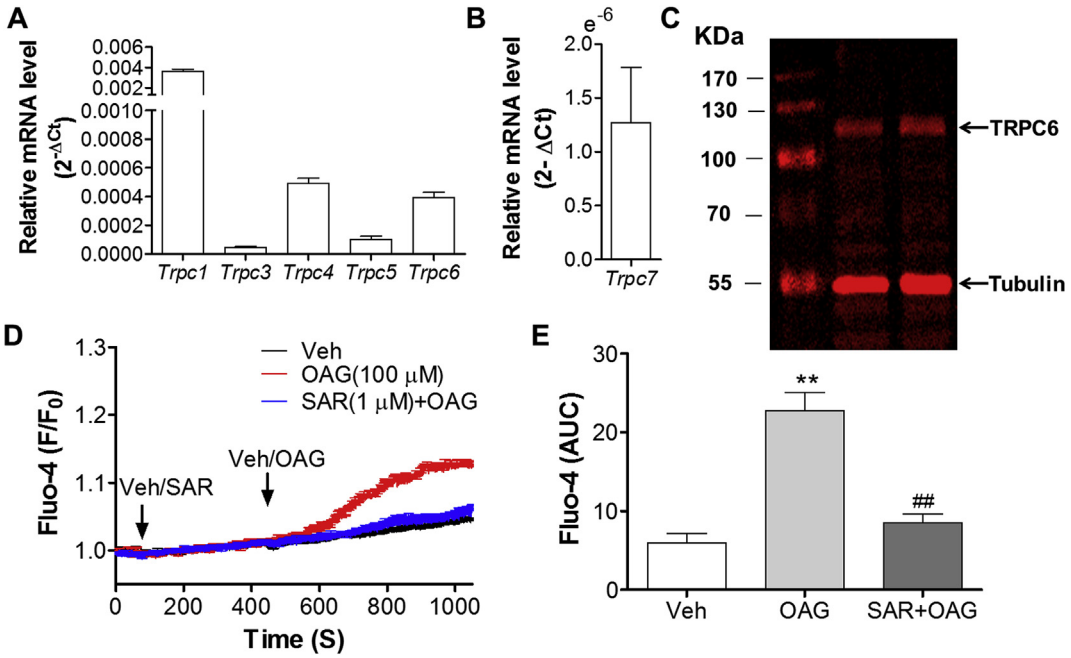

Fig. 3. Expression of TRPC channels in HK-2 cells. (A) Relative mRNA expression of TRPC channels in HK-2 cells. (B) TRPC7 expression in human keratinocytes at the mRNA level. (C) Representative western blots of TRPC6 expression in HK-2 cells. (D) Representative traces of OAG (100 μM) induced Ca^{2+} influx in the presence and absence of SAR7334 in HK-2 cells. (E) Quantitation of SAR7334 effect on OAG-induced Ca^{2+} influx in HK-2 cells. Area under curve (AUC) values were analysed from an epoch of 10 min following the addition of OAG. Each experiment was repeated twice, each in three replicates. Each data point represents mean ± S.E.M. **, $p < 0.01$, OAG *vs.* vehicle, ##, $p < 0.01$, SAR + OAG *vs.* OAG.

inhibitor, SAR7334 (Maier et al., 2015), suggesting the functional expression of TRPC6 channels in HK-2 cells (Fig. 3D&E).

3.4. Inhibition of TRPC6 channel activity suppressed CNCP-induced Ca^{2+} influx in HK-2 cells

Given the expression of many TRPC channels in HK-2 cells, we next examined whether inhibitors of TRPC channels were able to inhibit CNCP-induced Ca^{2+} influx. The TRPC3/6/7 inhibitor, SAR7734 (1 μM) dramatically suppressed the CNCP-induced Ca^{2+} response by 57.2% (Fig. 4A&B). However, a TRPC3 selective inhibitor, Pry3 (10 μM) (Kiyonaka et al., 2009), minimally affected the CNCP Ca^{2+} response (AUC values: 72.52 ± 5.85 *vs.* 76.71 ± 14.33, $p > 0.05$, n = 3) (Fig. 4C&D). Similarly, the TRPC1/4/5 inhibitor, Pico145 (100 nM) (Rubaiy et al., 2017), did not affect the CNCP-induced Ca^{2+} response (AUC values: 85.46 ± 3.71 *vs.* 76.71 ± 14.33, $p > 0.05$, n = 3) (Fig. 4C&D).

3.5. CNCP directly activated TRPC6 channels

We next examined whether CNCP can directly activate TRPC6 channels in a heterologous expression system. Whole cell recording revealed that CNCP increased TRPC6 currents in a concentration dependent manner at both positive (+100 mV) and negative (−100 mV) potentials in TRPC6-HEK-293 cells (Fig. 5A). CNCP elicited characteristic nonselective cation conductance with a reversal potential close to 0 mV and dually rectifying current-voltage relationships (Fig. 5B). SAR7344 inhibited both inward (−100 mV) and outward (+100 mV) currents induced by CNCP (Fig. 5A, B&D). The EC_{50} values for CNCP-induced TRPC6 currents at +100 mV and −100 mV were 6.01 μM (4.37–8.29, 95% CI) and 3.79 μM (2.44–5.90, 95% CI), respectively (Fig. 5C). Outside-out voltage patch recording showed that CNCP significantly increased the open probability (P_o) of TRPC6 channels from 0.050 ± 0.01 to 0.33 ± 0.08. A bath application of SAR7334 completely inhibited the CNCP-induced P_o increase of TRPC6 channels (Fig. 5E&F).

3.6. Inhibition of TRPC6 channel activity attenuated CNCP-induced cytotoxicity in HK-2 cells

Given that a TRPC6 inhibitor suppressed the CNCP-induced Ca^{2+} response, we examined whether the inhibition of TRPC6 ameliorated CNCP-induced toxicity in HK-2 cells. The pretreatment of cells with SAR7344 significantly decreased CNCP-induced cell death by 53.4% (Fig. 6A&B) and apoptosis by 48.7% (Fig. 6C&D).

3.7. CNCP increased caspase-3 activity

We next examined weather CNCP-induced HK-2 cell apoptosis was through caspase activity. CNCP (30 μM) exposure gradually increased cleaved caspase-3 levels, which reached a plateau at 4 h following CNCP exposure (Fig. 7A&B). Pretreatment with SAR7334 attenuated CNCP-induced caspase-3 activation by 64.1% (Fig. 7C&D).

4. Discussion

CNCP is a neolignan abundantly present in medicinal plants, including *K. lappacea* (Baumgartner et al., 2011b), a drug listed in the European Pharmacopoeia and the edible plants such as *P. regnellii* (Felipe et al., 2006), *R. diacanthum* Pall, and *R. manshuricum* (Maxim.) Kom. CNCP displays a variety of activities including insecticidal (Chauret et al., 1996), anti-fungal (De Campos et al., 2005), anti-

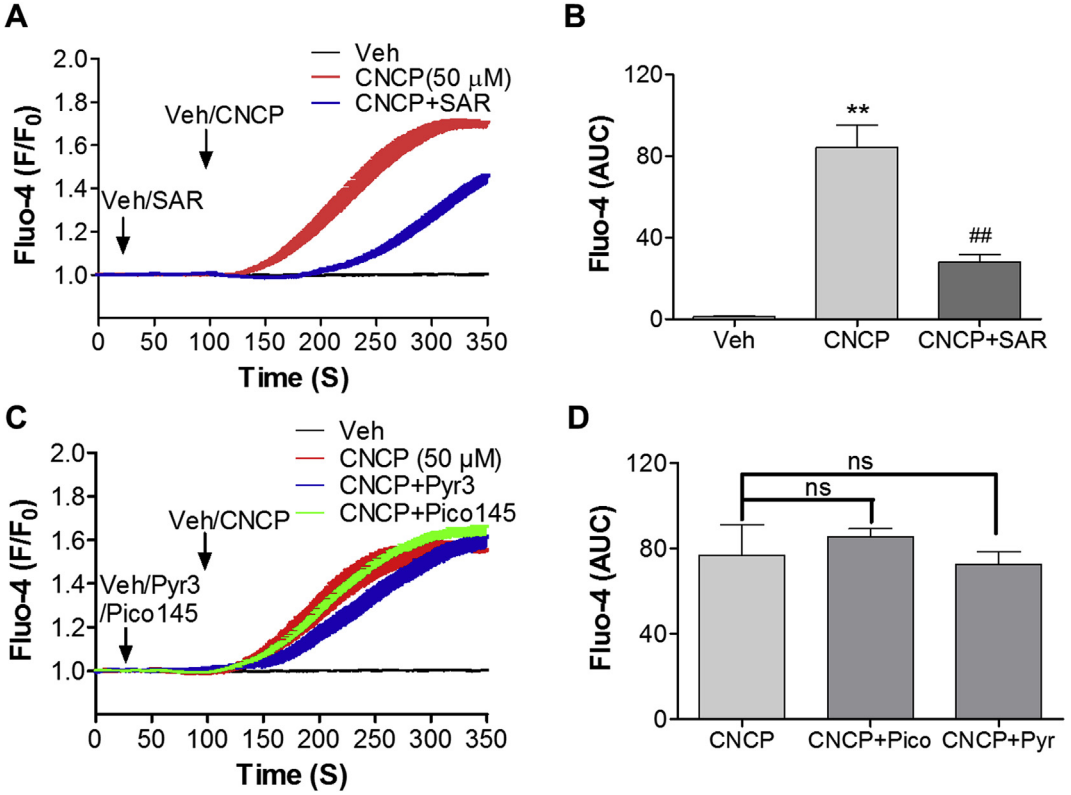

Fig. 4. Influence of SAR7334, Pyr3 or Pico145 on CNCP (50 μM) -induced Ca^{2+} influx in HK-2 cells. (A) Representative traces of CNCP induced $[Ca^{2+}]_i$ elevation in the presence or absence of SAR7334 (1 μM) in HK-2 cells. (B) Quantification of the effect of SAR7334 on CNCP evoked elevation of $[Ca^{2+}]_i$. (C) Representative traces of CNCP evoked $[Ca^{2+}]_i$ elevation in the presence or absence of Pico145 (100 nM) or Pyr3 (10 μM) in HK-2 cells. (E) Quantification of the effect of Pico145 and Pyr3 on CNCP evoked elevation of $[Ca^{2+}]_i$. Each experiment was performed three times each in triplicates. Each data point represents mean ± S.E.M. **, $p < 0.01$, CNCP *vs.* vehicle (0.1% DMSO), ##, $p < 0.01$, SAR + CNCP *vs.* CNCP.

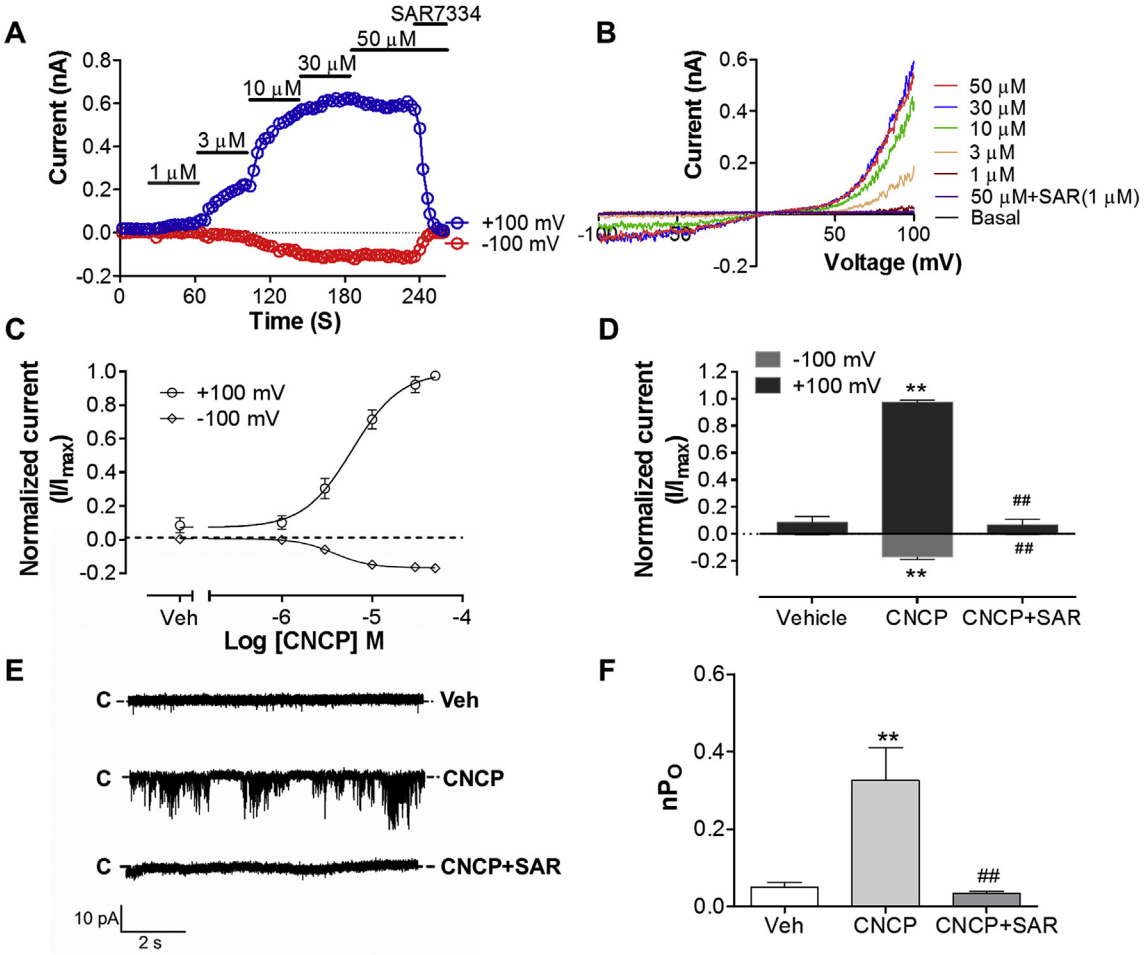

Fig. 5. CNCP evoked TRPC6 currents in TRPC6-HEK-293 cells. (A) Representative traces of whole cell currents at +100 mV and −100 mV potentials recorded before and after consecutive bath application of increasing concentrations of CNCP and SAR7334 (1 μM). (B) Current-voltage (I–V) relationships in the presence or absence of different concentrations of CNCP. (C) Concentration-response curves for CNCP-activated TRPC6 currents at both +100 mV and −100 mV potentials. (D) Quantification of SAR7334 (1 μM) effects on CNCP (50 μM)-induced TRPC6 currents at both +100 mV and −100 mV potentials. (F) Representative traces of outside-out recordings in HEK-293 cells expressing TRPC6 after exposure to vehicle (top trace), CNCP (50 μM) (middle trace) and CNCP + SAR7334 (1 μM, bottom trace). The voltage was clamped at −80 mV potential. (E) Quantification of TRPC6 channel open probability (nP_o) after exposure to vehicle, CNCP and CNCP + SAR7334. Each data point represents mean ± S.E.M. (n ≥ 4 cells). **, $p < 0.01$, CNCP *vs.* vehicle, ##, $p < 0.01$, CNCP + SAR7334 *vs.* CNCP.

trypanosomal (Luize et al., 2006), anti-tuberculotic (Scodro et al., 2013), anti-nociceptive and anti-inflammatory activities (Da Silva et al., 2010). CNCP has also been demonstrated to display antioxidative and photoprotective activities in rat erythrocytes and human keratinocytes with IC_{50} values of 2.5 μM and 12.3 μM, respectively (Carini et al., 2002). However, in the current study, we demonstrated that CNCP-induced apoptotic cell death in HK-2 cells, suggesting the potential renal toxicity of CNCP as a therapeutic agent. We also demonstrated that the activation of TRPC6 contributed to CNCP-induced apoptosis in HK-2 cells (see discussion below). It is possible that the tissue-dependent expression of TRPC6 may be responsible for this discrepancy (Abramowitz and Birnbaumer, 2009; Sawamura et al., 2016; Zhang et al., 2014).

Intracellular Ca^{2+} acts as a second messenger to regulate diverse cellular functions such as the cell cycle, DNA synthesis, and cell proliferation, differentiation, and death (Berridge et al., 1998, 2000; Clapham, 2007; Zhivotovsky and Orrenius, 2011). The overloading of $[Ca^{2+}]_i$ leads to necrosis and/or apoptosis, depending on the cell type (Orrenius et al., 2003; Rizzuto et al., 2003; Zhivotovsky and Orrenius, 2011). We demonstrated that CNCP induces a rapid and sustained elevation of $[Ca^{2+}]_i$ in HK-2 cells, suggesting that CNCP-induced apoptotic cell death in HK-2 cells was a consequence of $[Ca^{2+}]_i$ overloading. Overloading of $[Ca^{2+}]_i$ can result from augmented extracellular Ca^{2+} influx through a variety of Ca^{2+} permeable ion channels (Carafoli et al., 2001; Szydlowska and Tymianski, 2010) or from enhanced Ca^{2+} release from intracellular Ca^{2+} stores (Gorlach et al., 2006; Marks, 1997). In extracellular buffer without Ca^{2+} (with 1 mM EGTA), CNCP-induced a much smaller Ca^{2+} response than what was observed in the physiological buffer with a Ca^{2+} concentration of 2.3 mM. Moreover, in the extracellular buffer without Ca^{2+} (with 1 mM EGTA), the depletion of intracellular Ca^{2+} stores with TG abolished the CNCP-induced Ca^{2+} response. Considered together, these data demonstrate that both extracellular Ca^{2+} influx and Ca^{2+} release from intracellular Ca^{2+} stores were involved in the CNCP-induced Ca^{2+} response.

Although we were not able to delineate the molecular target(s) of CNCP-induced Ca^{2+} release from intracellular Ca^{2+} stores, we demonstrated that CNCP-induced Ca^{2+} influx was mediated by TRPC6. TRPCs are a class of Ca^{2+}-permeable, nonselective cation channels expressed in many cell types (Abramowitz and Birnbaumer, 2009; Sawamura et al., 2016; Zhang et al., 2014). Many studies have demonstrated the importance of TRPCs on kidney pathophysiology. Gain-of-function mutations in TRPC6 channels in patients with FSGS enhance Ca^{2+} influx into podocytes with subsequent destruction of glomerular filtration barrier (Dryer and Reiser, 2010; Reiser et al., 2005; Winn et al., 2005). In the current study, we observed the mRNA expression of

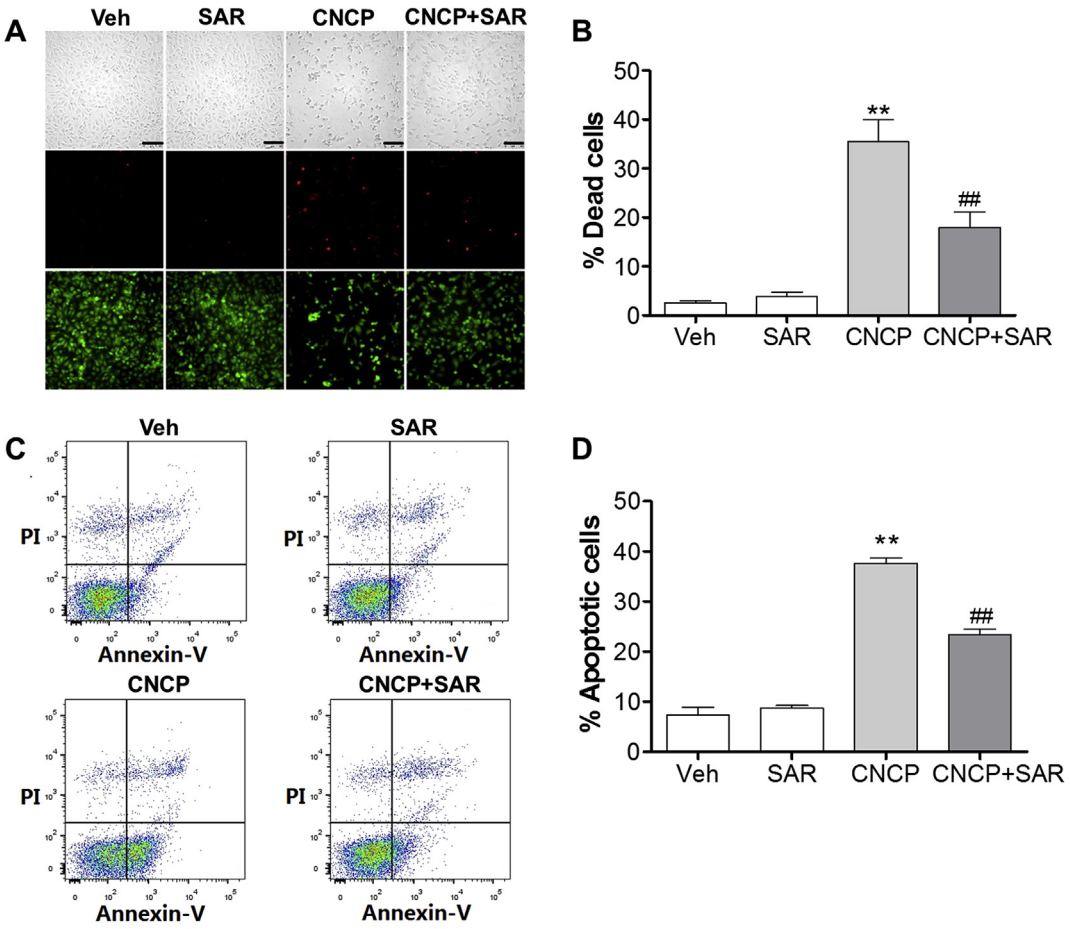

Fig. 6. SAR7334 suppressed CNCP-induced HK-2 cell death. (A) Representative images for FDA and PI double stained HK-2 cells exposed to 0.1% DMSO or CNCP (30 μM) for 24 h in the presence or absence of SAR7334 (1 μM). Scale bar = 100 μm. (B) Quantification of the effect of SAR7334 on CNCP (30 μM)-induced HK-2 cell death. (C) Representative flow cytometry diagrams after 2 h exposure with 0.1% DMSO or CNCP (30 μM) in the presence or absence of SAR7334 (1 μM). (D) SAR7334 (1 μM) suppressed CNCP-induced apoptosis. Each experiment was repeated three times, each in triplicates. Each data point represents mean ± S.E.M. **, $p < 0.01$, CNCP vs. vehicle, $^{\#\#}$, $p < 0.01$, SAR + CNCP *vs.* CNCP.

TRPC1-6 but not TRPC7 in HK-2 cells. SAR 7334, a TRPC3/6/7 inhibitor, inhibited CNCP-induced Ca^{2+} response while Pyr3, a TRPC3 inhibitor, and Pico145, a TRPC1/4/5 inhibitor had little effect, suggesting that CNCP-induced Ca^{2+} influx was mediated by TRPC6 channel activity. It has been demonstrated that TRPC6 channels are involved in neonatal glomerular mesangial cell apoptosis by the activation of the calcineurin-NFAT pathway (Schloendorff et al., 2009). The pharmacological inhibition or genetic ablation of TRPC6 channels suppresses oxidative stress induced apoptosis in renal proximal tubular cells (Hou et al., 2018). In agreement with previous studies, we also demonstrated that CNCP-induced HK-2 apoptosis was inhibited by TRPC6 inhibition.

TRPC6 channels can be activated by diacylglycerol (DAG), a lipid second messenger that is mainly formed by cleavage of phosphatidylinositol-4,5-bisphosphate by phosphatidylinositol-specific phospholipases as a consequence of Gq-protein coupled receptor (GPCR) activation (Hofmann et al., 1999). CNCP activated TRPC6 channels by increasing the open probability in a heterologous expression system, suggesting the direct activation of TRPC6 channels but not enhanced Gq-coupled signalling pathways was responsible for CNCP-induced $[Ca^{2+}]_i$ elevation and apoptotic death in HK-2 cells. It should be noted that although OAG, an analogue of DAG, was capable of inducing Ca^{2+} influx in HK-2 cells, OAG was not able to trigger apoptosis in HK-2 cells (Supplemental Figure 1). Whether CNCP-induced Ca^{2+} release from intracellular Ca^{2+} stores can facilitate CNCP-induced apoptosis in HK-2 cells needs further investigation. Another explanation is that CNCP-induced Ca^{2+} influx is much more robust than that of OAG in HK-2 cells.

In summary, we demonstrated that CNCP, a neolignan that is found in high levels in several medical plants, triggered apoptotic cell death through caspase-3 activation. We further demonstrated that CNCP elevated $[Ca^{2+}]_i$ through both Ca^{2+} release from intracellular Ca^{2+} stores and extracellular Ca^{2+} influx. Moreover, we demonstrated that the direct activation of TRPC6 channels contributed to CNCP-induced Ca^{2+} influx and apoptotic cell death in HK-2 cells. Our data not only show the potential risk of using CNCP or medical plants containing CNCP as therapeutic agents but also demonstrate a novel mechanism that apoptotic cell death in HK-2 cells through the activation of caspase-3 due to the activation of TRPC6. Given the efficacious response of CNCP on endogenously expressed TRPC6 channels, CNCP may represent a useful tool to probe the function of TRPC6 channels.

Conflicts of interests

The authors declare no conflict of interests.

Author contributions

Experimental design: ZC and CC.
Experimentation: GY, HM, YW, and BZ.
Data analysis: GY, HM, YW, and CZ.
Paper writing: GY, CC, and ZC.

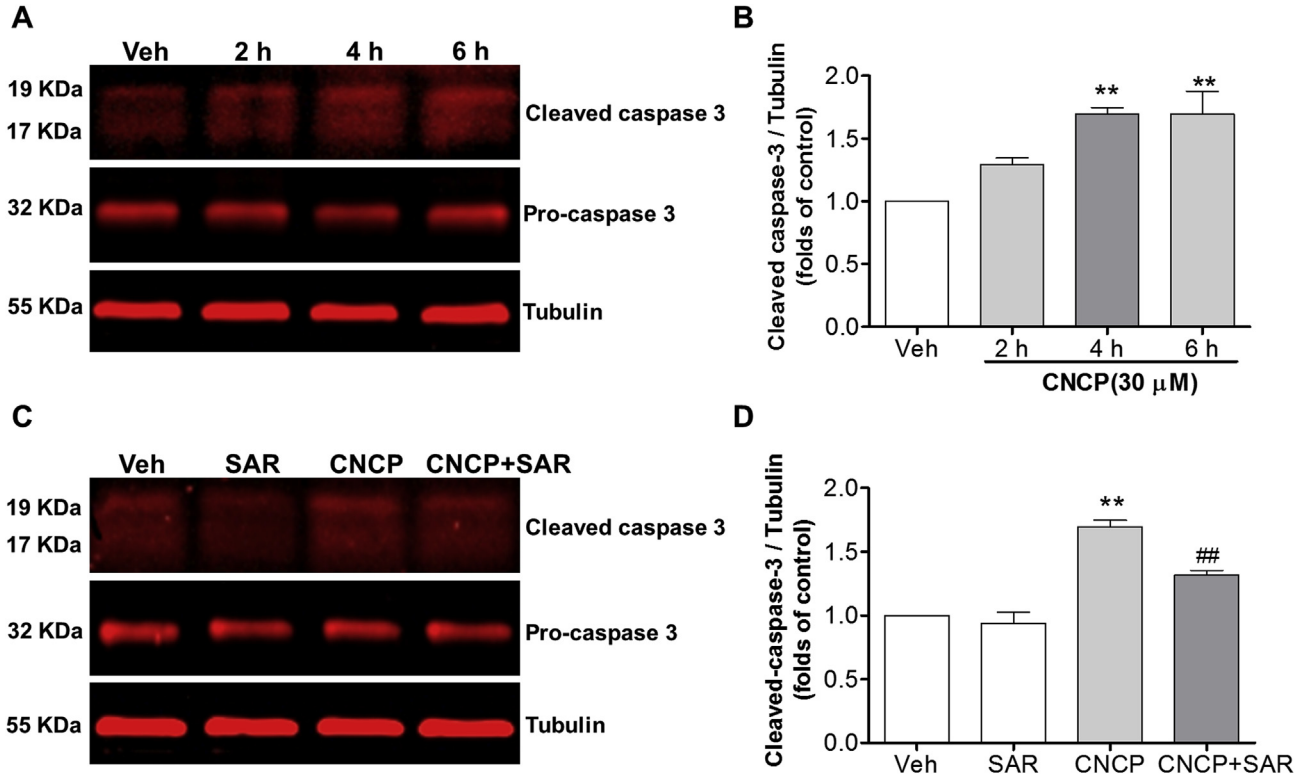

Fig. 7. Influence of SAR7334 on CNCP induced caspase-3 activation. (A) Representative western blots showing CNCP (30 μM)-activated caspase 3 at 2 h, 4 h, 6 h. Beta-tubulin was used as an internal control. (B) Quantification of CNCP-induced caspase-3 activation. (C) Representative western blots of CNCP-activated caspase 3 at 4 h in the presence or absence of SAR7334. (D) Quantification of the effect of SAR7334 on CNCP-induced caspase-3 activation. Each data point represents mean ± S.E.M. from two experiments, each in duplicates. **, $p < 0.01$, CNCP vs. vehicle, ##, $p < 0.01$, CNCP + SAR7334 *vs.* CNCP.

Declaration of interests

The authors declare that they have no known competing financial interests or personal relationships that could have appeared to influence the work reported in this paper.

Acknowledgements

This work was supported by the National Natural Science Foundation of China (Nos. 81603389, 21777192); the National Science and Technology Major Projects for “Major New Drugs Innovation and Development” (No. 2018ZX09101003-004-002); the Natural Science Foundation of Jiangsu Province (CN) (No. BK20160754) and the “Double First-Class” project of China Pharmaceutical University (No. CPU2018GY18).

Appendix A. Supplementary data

Supplementary data to this article can be found online at https://doi.org/10.1016/j.fct.2019.04.061.

Transparency document

Transparency document related to this article can be found online at https://doi.org/10.1016/j.fct.2019.04.061.

References

Abramowitz, J., Birnbaumer, L., 2009. Physiology and pathophysiology of canonical transient receptor potential channels. FASEB J. 23, 297–328.
Baumgartner, L., Schwaiger, S., Stuppner, H., 2011a. Quantitative analysis of anti-inflammatory lignan derivatives in Ratanhiae radix and its tincture by HPLC-PDA and HPLC-MS. J. Pharm. Biomed. Anal. 56, 546–552.
Baumgartner, L., Sosa, S., Atanasov, A.G., Bodensieck, A., Fakhrudin, N., Bauer, J., Favero, G.D., Ponti, C., Heiss, E.H., Schwaiger, S., Ladurner, A., Widowitz, U., Loggia, R.D., Rollinger, J.M., Werz, O., Bauer, R., Dirsch, V.M., Tubaro, A., Stuppner, H., 2011b. Lignan derivatives from Krameria lappacea roots inhibit acute inflammation in vivo and pro-inflammatory mediators in vitro. J. Nat. Prod. 74, 1779–1786.
Berridge, M.J., Bootman, M.D., Lipp, P., 1998. Calcium - a life and death signal. Nature 395, 645–648.
Berridge, M.J., Lipp, P., Bootman, M.D., 2000. The versatility and universality of calcium signalling. Nat. Rev. Mol. Cell Biol. 1, 11–21.
Cao, G.Y., Xu, W., Yang, X.W., Gonzalez, F.J., Li, F., 2015. New neolignans from the seeds of Myristica fragrans that inhibit nitric oxide production. Food Chem. 173, 231–237.
Carafoli, E., Santella, L., Branca, D., Brini, M., 2001. Generation, control, and processing of cellular calcium signals. Crit. Rev. Biochem. Mol. Biol. 36, 107–260.
Carini, M., Aldini, G., Orioli, M., Facino, R.M., 2002. Antioxidant and photoprotective activity of a lipophilic extract containing neolignans from Krameria triandra roots. Planta Med. 68, 193–197.
Chauret, D.C., Bernard, C.B., Arnason, J.T., Durst, T., Krishnamurty, H.G., SanchezVindas, P., Moreno, N., SanRoman, L., Poveda, L., 1996. Insecticidal neolignans from Piper decurrens. J. Nat. Prod. 59, 152–155.
Chen, C.-y., Weisel, M., 2013. Concise asymmetric synthesis of (+)-Conocarpan and obtusafuran. Synlett 24, 189–192.
Chen, T., Li, C., Li, Y., Yi, X., Lee, S.M., Zheng, Y., 2016. Oral delivery of a nanocrystal formulation of schisantherin a with improved bioavailability and brain delivery for the treatment of Parkinson's disease. Mol. Pharm. 13, 3864–3875.
Clapham, D.E., 2007. Calcium signaling. Cell 131, 1047–1058.
Da Silva, R.Z., Yunes, R.A., de Souza, M.M., Delle Monache, F., Cechinel-Filho, V., 2010. Antinociceptive properties of conocarpan and orientin obtained from Piper solmsianum C. DC. var. solmsianum (Piperaceae). J. Nat. Med. 64, 402–408.
De Campos, M.P., Cechinel, V., Da Silva, R.Z., Yunes, R.A., Zacchino, S., Juarez, S., Cruz, R.C., Cruz, A.B., 2005. Evaluation of antifungal activity of Piper solmsianum C. DC. var. solmsianum (Piperaceae). Biol. Pharm. Bull. 28, 1527–1530.
Dryer, S.E., Reiser, J., 2010. TRPC6 channels and their binding partners in podocytes: role in glomerular filtration and pathophysiology. Am. J. Physiol. Renal. Physiol. 299, F689–F701.
Felipe, D.F., Filho, B.P., Nakamura, C.V., Franco, S.L., Cortez, D.A., 2006. Analysis of neolignans compounds of Piper regnellii (Miq.) C. DC. var. pallescens (C. DC.) Yunck by HPLC. J. Pharm. Biomed. Anal. 41, 1371–1375.
Gao, Q., Yang, M.B., Zuo, Z., 2018. Overview of the anti-inflammatory effects, pharmacokinetic properties and clinical efficacies of arctigenin and arctiin from Arctium lappa L. Acta Pharmacol. Sin. 39, 787–801.
Giglio, R.V., Patti, A.M., Cicero, A.F.G., Lippi, G., Rizzo, M., Toth, P.P., Banach, M., 2018. Polyphenols: potential use in the prevention and treatment of cardiovascular diseases. Curr. Pharmaceut. Des. 24, 239–258.

Gorlach, A., Klappa, P., Kietzmann, T., 2006. The endoplasmic reticulum: folding, calcium homeostasis, signaling, and redox control. Antioxidants Redox Signal. 8, 1391–1418.
Gu, L., Wang, Y., Yang, G., Tilyek, A., Li, S., Yu, B., Chai, C., Cao, Z., 2018. Ribes diacanthum Pall (RDP) ameliorates UUO-induced renal fibrosis via both canonical and non-canonical TGF-beta signaling pathways in mice. J. Ethnopharmacol. 231, 302–310.
Hayashi, T., Thomson, R.H., 1975. New lignans in Conocarpus erectus. Phytochemistry 14, 1085–1087.
He, Y., Zou, X., Li, X., Chen, J., Jin, L., Zhang, F., Yu, B., Cao, Z., 2017. Activation of sodium channels by alpha-scorpion toxin, BmK NT1, produced neurotoxicity in cerebellar granule cells: an association with intracellular Ca(2+) overloading. Arch. Toxicol. 91, 935–948.
Hofmann, T., Obukhov, A.G., Schaefer, M., Harteneck, C., Gudermann, T., Schultz, G., 1999. Direct activation of human TRPC6 and TRPC3 channels by diacylglycerol. Nature 397, 259–263.
Hou, X., Xiao, H., Zhang, Y., Zeng, X., Huang, M., Chen, X., Birnbaumer, L., Liao, Y., 2018. Transient receptor potential channel 6 knockdown prevents apoptosis of renal tubular epithelial cells upon oxidative stress via autophagy activation. Cell Death Dis. 9, 1015.
Jeong, E.J., Lee, H.K., Lee, K.Y., Jeon, B.J., Kim, D.H., Park, J.H., Song, J.H., Huh, J., Lee, J.H., Sung, S.H., 2013. The effects of lignan-riched extract of Shisandra chinensis on amyloid-beta-induced cognitive impairment and neurotoxicity in the cortex and hippocampus of mouse. J. Ethnopharmacol. 146, 347–354.
Kim, K.H., Moon, E., Kim, S.Y., Leet, K.R., 2010. Lignans from the tuber-barks of colocasia antiquorum var. esculenta and their antimelanogenic activity. J. Agric. Food Chem. 58, 4779–4785.
Kiyonaka, S., Kato, K., Nishida, M., Mio, K., Numaga, T., Sawaguchi, Y., Yoshida, T., Wakamori, M., Mori, E., Numata, T., Ishii, M., Takemoto, H., Ojida, A., Watanabe, K., Uemura, A., Kurose, H., Morii, T., Kobayashi, T., Sato, Y., Sato, C., Hamachi, I., Mori, Y., 2009. Selective and direct inhibition of TRPC3 channels underlies biological activities of a pyrazole compound. Proc. Natl. Acad. Sci. U.S.A. 106, 5400–5405.
Li, Y., Zhou, B., Zhang, W., Yang, G., Zhang, C., Cao, Z., 2018. Chemical constituents from aerial parts of Ribes mandshuricum. Chin. Tradit. Herb. Drugs 49, 772–779.
Ligaa, U.D.B., Ninjil, N., 2006. Medicinal Plants of Mongolia Used in Western and Eastern Medicine. JKC Printing: Ulaanbaatar Mongolia, pp. 374.
Luize, P.S., Ueda-Nakamura, T., Dias Filho, B.P., Garcia Cortez, D.A., Nakamura, C.V., 2006. Activity of neolignans isolated from Piper regnellii (MIQ.) C. DC. var. pallescens (C. DC.) YUNCK against Trypanosoma cruzi. Biol. Pharm. Bull. 29, 2126–2130.
Ma, S.T., Liu, D.L., Deng, J.J., Niu, R., Liu, R.B., 2013. Effect of arctiin on glomerular filtration barrier damage in STZ-induced diabetic nephropathy rats. Phytother Res. 27, 1474–1480.
Maier, T., Follmann, M., Hessler, G., Kleemann, H.W., Hachtel, S., Fuchs, B., Weissmann, N., Linz, W., Schmidt, T., Lohn, M., Schroeter, K., Wang, L., Rutten, H., Strubing, C., 2015. Discovery and pharmacological characterization of a novel potent inhibitor of diacylglycerol-sensitive TRPC cation channels. Br. J. Pharmacol. 172, 3650–3660.
Marks, A.R., 1997. Intracellular calcium-release channels: regulators of cell life and death. Am. J. Physiol. 272, H597–H605.
Orrenius, S., Zhivotovsky, B., Nicotera, P., 2003. Regulation of cell death: the calcium-apoptosis link. Nat. Rev. Mol. Cell Biol. 4, 552–565.
Parhira, S., Yang, Z.F., Zhu, G.Y., Chen, Q.L., Zhou, B.X., Wang, Y.T., Liu, L., Bai, L.P., Jiang, Z.H., 2014. In vitro anti-influenza virus activities of a new lignan glycoside from the latex of Calotropis gigantea. PLoS One 9, e104544.
Pessini, G.L., Dias, B.P., Nakamura, C.V., Cortez, D.A.G., 2003. Antibacterial activity of extracts and neolignans from Piper regnellii (Miq.) C. DC. var. pallescens (C. DC.). Yunck. Mem. Inst. Oswaldo Cruz 98, 1115–1120.
Qu, C., Ding, M., Zhu, Y., Lu, Y., Du, J., Miller, M., Tian, J., Zhu, J., Xui, J., Wen, M., Er-Bu, A., Wan, J., Xiao, Y., Wu, M., McManus, O.B., Li, M., Wu, J., Luo, H.-R., Cao, Z., Shen, B., Wang, H., Zhu, M.X., Hong, X., 2017. Pyrazolopyrimidines as potent stimulators for transient receptor potential canonical 3/6/7 channels. J. Med. Chem. 60, 4680–4692.
Reiser, J., Polu, K.R., Moller, C.C., Kenlan, P., Altintas, M.M., Wei, C.L., Faul, C., Herbert, S., Villegas, I., Avila-Casado, C., McGee, M., Sugimoto, H., Brown, D., Kalluri, R., Mundel, P., Smith, P.L., Clapham, D.E., Pollak, M.R., 2005. TRPC6 is a glomerular slit diaphragm-associated channel required for normal renal function. Nat. Genet. 37, 739–744.
Rizwan, S., Naqshbandi, A., Farooqui, Z., Khan, A.A., Khan, F., 2014. Protective effect of dietary flaxseed oil on arsenic-induced nephrotoxicity and oxidative damage in rat kidney. Food Chem. Toxicol. 68, 99–107.
Rizzuto, R., Pinton, P., Ferrari, D., Chami, M., Szabadkai, G., Magalhaes, P.J., Di Virgilio, F., Pozzan, T., 2003. Calcium and apoptosis: facts and hypotheses. Oncogene 22, 8619–8627.
Rubaiy, H.N., Ludlow, M.J., Henrot, M., Gaunt, H.J., Miteva, K., Cheung, S.Y., Tanahashi, Y., Hamzah, N., Musialowski, K.E., Blythe, N.M., Appleby, H.L., Bailey, M.A., McKeown, L., Taylor, R., Foster, R., Waldmann, H., Nussbaumer, P., Christmann, M., Bon, R.S., Muraki, K., Beech, D.J., 2017. Picomolar, selective, and subtype-specific small-molecule inhibition of TRPC1/4/5 channels. J. Biol. Chem. 292, 8158–8173.
Saliba, Y., Karam, R., Smayra, V., Aftimos, G., Abramowitz, J., Birnbaumer, L., Fares, N., 2015. Evidence of a role for fibroblast transient receptor potential canonical 3 Ca2+ channel in renal fibrosis. J. Am. Soc. Nephrol. 26, 1855–1876.
Sawamura, S., Hatano, M., Takada, Y., Hino, K., Kawamura, T., Tanikawa, J., Nakagawa, H., Hase, H., Nakao, A., Hirano, M., Rotrattanadumrong, R., Kiyonaka, S., Mori, M.X., Nishida, M., Hu, Y., Inoue, R., Nagata, R., Mori, Y., 2016. Screening of transient receptor potential canonical channel activators identifies novel neurotrophic piperazine compounds. Mol. Pharmacol. 89, 348–363.
Schloendorff, J., del Camino, D., Carrasquillo, R., Lacey, V., Pollak, M.R., 2009. TRPC6 mutations associated with focal segmental glomerulosclerosis cause constitutive activation of NFAT-dependent transcription. Am. J. Physiol. Cell Physiol. 296, C558–C569.
Scodro, R.B.L., Pires, C.T.A., Carrara, V.S., Lemos, C.O.T., Cardozo-Filho, L., Souza, V.A., Correa, A.G., Siqueira, V.L.D., Lonardoni, M.V.C., Cardoso, R.F., Cortez, D.A.G., 2013. Anti-tuberculosis neolignans from Piper regnellii. Phytomedicine 20, 600–604.
Silva, A.R., Polo, E.C., Martins, N.C., Correia, C.R.D., 2018. Enantioselective oxy-heck-matsuda arylations: expeditious synthesis of dihydrobenzofuran systems and total synthesis of the neolignan (-)-Conocarpan. Adv. Synth. Catal. 360, 346–365.
Stojakowska, A., Michalska, K., Malarz, J., Beharav, A., Kisiel, W., 2013. Root tubers of Lactuca tuberosa as a source of antioxidant phenolic compounds and new furofuran lignans. Food Chem. 138, 1250–1255.
Szydlowska, K., Tymianski, M., 2010. Calcium, ischemia and excitotoxicity. Cell Calcium 47, 122–129.
Teponno, R.B., Kusari, S., Spiteller, M., 2016. Recent advances in research on lignans and neolignans. Nat. Prod. Rep. 33, 1044–1092.
Tilyek, A., Chai, C., Hou, X., Zhou, B., Zhang, C., Cao, Z., Yu, B., 2016. The protective effects of Ribes diacanthum Pall on cisplatin-induced nephrotoxicity in mice. J. Ethnopharmacol. 178, 297–306.
Winn, M.P., Conlon, P.J., Lynn, K.L., Farrington, M.K., Creazzo, T., Hawkins, A.F., Daskalakis, N., Kwan, S.Y., Ebersviller, S., Burchette, J.L., Pericak-Vance, M.A., Howell, D.N., Vance, J.M., Rosenberg, P.B., 2005. A mutation in the TRPC6 cation channel causes familial focal segmental glomerulosclerosis. Science 308, 1801–1804.
Wu, Y.L., Xie, J., An, S.W., Oliver, N., Barrezueta, N.X., Lin, M.H., Birnbaumer, L., Huang, C.L., 2017. Inhibition of TRPC6 channels ameliorates renal fibrosis and contributes to renal protection by soluble klotho. Kidney Int. 91, 830–841.
Zhang, H., Li, W., Xue, Y., Zou, F., 2014. TRPC1 is involved in Ca(2)(+) influx and cytotoxicity following Pb(2)(+) exposure in human embryonic kidney cells. Toxicol. Lett. 229, 52–58.
Zheng, S.L., Yu, W.Y., Xu, M.X., Che, C.M., 2003. First synthesis of naturally occurring (+/-)-epi-conocarpan. Tetrahedron Lett. 44, 1445–1447.
Zhivotovsky, B., Orrenius, S., 2011. Calcium and cell death mechanisms: a perspective from the cell death community. Cell Calcium 50, 211–221.
Zhou, B., Wang, Y., Zhang, C., Yang, G., Zhang, F., Yu, B., Chai, C., Cao, Z., 2018. Ribemansides a and B, TRPC6 inhibitors from Ribes manshuricum that suppress TGF-beta1-induced fibrogenesis in HK-2 cells. J. Nat. Prod. 81, 913–917.
Zhou, B., Zhang, C., Zou, X., Xu, J., Li, Y., Li, X., Chai, C., Cao, Z., 2016. Chemical constituents from the aerial parts of Ribes diacanthum Pall. Chin. Pharmaceut. J. 21, 1918–1922.
Zou, X., Wu, Y., Chen, J., Zhao, F., Zhang, F., Yu, B., Cao, Z., 2017. Activation of sodium channel by a novel alpha-scorpion toxin, BmK NT2, stimulates ERK1/2 and CERB phosphorylation through a Ca(2+) dependent pathway in neocortical neurons. Int. J. Biol. Macromol. 104, 70–77.
Zuniga-Toala, A., Zatarain-Barron, Z.L., Hernandez-Pando, R., Negrette-Guzman, M., Huerta-Yepez, S., Torres, I., Pinzon, E., Tapia, E., Pedraza-Chaverri, J., 2013. Nordihydroguaiaretic acid induces Nrf2 nuclear translocation in vivo and attenuates renal damage and apoptosis in the ischemia and reperfusion model. Phytomedicine 20, 775–779.